

Multi-fold Non-Hermitian Phase Transitions and Exact Solution of Non-Hermitian Skin Effects

Xintong Zhang, Xiaoxiao Song, Shubo Zhang, Tengfei Zhang, Yuanjie Liao, Xinyi Cai, and Jing Li*

Department of Optical Science and Engineering, Shanghai Ultra-Precision Optical Manufacturing Engineering Center, Fudan University, Shanghai 200433, China

(Dated: June 24, 2022)

Non-Hermitian systems can exhibit extraordinary sensitivity to boundary conditions, where the localized topological boundary modes and the non-Hermitian skin effects can coexist or individually appear, leading to the non-Hermitian four-fold phase transitions. Several efforts have been made to reconstruct the non-Hermitian bulk-boundary correspondence, but it is still challenging to present the four-fold phase diagram more quickly. Here, we directly give the exact expression of four-fold phase-transition point without any numerical calculation in the parameter space, through the combination of exact solution approach and non-Hermitian winding numbers. Our exact solution approach not only characterizes the energy and penetration length of skin modes, but also unveils the intrinsic difference between the topological modes and skin modes. To illustrate the general benefits of our methods, a more complicated non-Hermitian Su-Schrieffer-Heeger chain with long-range couplings and a modified Lee model without sub-lattice symmetry are investigated, providing a general routine to study various non-Hermitian phases.

I. INTRODUCTION

Band topology in non-Hermitian physics has attracted intensive studies recently[1–7]. As is well-known for Hermitian systems, a nontrivial Bloch band invariant implies the emergency of topological boundary modes under open boundary condition (OBC)[8, 9], which can date back to the discovery of integer quantum Hall effect[10–12]. However, similar bulk-boundary correspondence appears to be violated in non-Hermitian regimes. On one hand, the spectrum in open system is far different from that in periodic system, especially the topological phase transition points are not equivalent to the bulk gap-closing points[13, 14]. On the other hand, such a non-consistency of spectra always comes along with the non-Hermitian skin effect (NHSE) phenomenon[15–19], where all the eigenstates under OBC are exponentially localized at the boundary of the lattice. These phenomena extend the richness of the phase transitions, and provide higher reconfigurability in non-Hermitian classical systems or quantum systems, such as photonics[20–22], electrical circuits[23–27], acoustics[28], and quantum-walk dynamics[29], which are beyond any known phenomenon from their Hermitian counterparts.

Several efforts have been made to restore the bulk-boundary correspondence in non-Hermitian systems[30–45]. With regard to the prediction of non-Hermitian topological boundary modes, one approach is the non-Bloch-wave approach, including the generalized Brillouin Zone (GBZ) method[32–36], and its equivalent form called non-Hermitian winding numbers[37–39], which transform the constraint on boundary condition into the imaginary part of wave vector. Another approach is the biorthogonal polarization method[40–42], which

establishes the mapping relation between broken lattice topology and unbroken lattice topology, and the biorthogonality of non-Hermitian eigenstates is used to simplify the derivation. With regard to NHSE, the eigenstates can be quantitatively analyzed through exact solution approach[43, 44], which rigorously shows how the boundary condition and lattice size affect the eigenstates. Meanwhile, transfer-matrix method[45] can explain the correspondence between NHSE and non-consistency of spectra. However, since the topological modes and skin modes can coexist or individually appear, it is still challenging to present the non-Hermitian four-fold phase diagram quickly in a more complicated non-Hermitian system. For example, the prediction by GBZ method relies on the numerical calculation on the routine of generalized Brillouin Zone, at each point of parameter space.

In this work, we focused on the problem that how to present the non-Hermitian four-fold phase diagram more quickly, for further flexible regulation in a more complicated non-Hermitian system. To address this issue, a non-Hermitian Su-Schrieffer-Heeger (SSH) chain with long-range couplings is proposed. We developed the non-Hermitian winding numbers and exact solution approach in this model, and then both the existence condition of topological modes and skin modes are analytically expressed. Therefore, the four-fold phase diagram is quickly established by the combination of these two methods, without any numerical calculation in the parameter space. Additionally, by the exact solution approach, the intrinsic difference between topological modes and skin modes is uncovered, and we also found that our lattice model behaves like a Hermitian system under the protection of pseudo-Hermitian symmetry. To illustrate the general benefits of our exact solution approach, a modified Lee model without sub-lattice symmetry is also investigated. Our research on the multi-fold non-Hermitian phase transitions provides a general tool to study various non-Hermitian boundary behaviors.

* lijing@fudan.edu.cn

II. RESULTS AND DISCUSSION

A. Four-fold Non-Hermitian Phase Transitions

Here, we demonstrated the numerical results on the four-fold non-Hermitian phase transitions in a more complicated non-Hermitian SSH chain with long-range couplings, as shown in Fig. 1. The real-space Hamiltonian

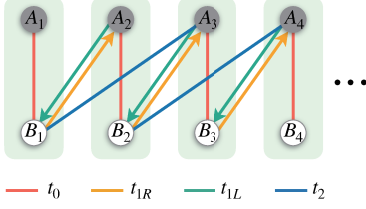


FIG. 1. **Schematic view of the one-dimensional non-Hermitian lattice model with long-range couplings.** The green blocks imply the position of unit cells, and each contains two sites A and B . $t_{1R,1L}$ are the non-reciprocal nearest inter-cell interaction, while t_0 and t_2 are the reciprocal intra-cell and next-nearest inter-cell interaction.

under OBC is described as,

$$\hat{H} = \sum_{n=1}^N [\varepsilon_0 (c_{n,A}^\dagger c_{n,A} + c_{n,B}^\dagger c_{n,B}) + (t_0 c_{n,A}^\dagger c_{n,B} + h.c.)] + \sum_{n=1}^{N-1} t_{1R} c_{n+1,A}^\dagger c_{n,B} + t_{1L} c_{n,B}^\dagger c_{n+1,A} + \sum_{n=1}^{N-2} (t_2 c_{n+2,A}^\dagger c_{n,B} + h.c.), \quad (1)$$

where N is the number of the lattice unit cells, and each cell contains two inequivalent sites A and B with on-site energy ε_0 . t_0 and $t_{1R,1L}$ represent the intra-cell and nearest inter-cell interaction, and the non-Hermiticity origins from the non-reciprocity that $t_{1R} \neq t_{1L}^*$. Notably, next-nearest inter-cell interaction t_2 is added to enhance the tunability in this model.

Figure 2 illustrates the observation of four-fold phase transitions in our non-Hermitian model. As shown in Fig. 2(a) for phase I, the topological boundary modes with eigenvalues $E = \varepsilon_0$ appear but the skin modes vanish, while for phase II shown in Fig. 2(b), both the topological modes and skin modes can appear simultaneously. As shown in Fig. 2(c) for phase III, only the skin modes survive, and all the eigenstates are localized at $n = 1$ side of the lattice. Phase IV shown in Fig. 2(d) illustrates the trivial phase without either of the boundary behaviors.

B. Non-Hermitian winding numbers

To restore the non-Hermitian bulk-boundary correspondence and establish the four-fold phase transition

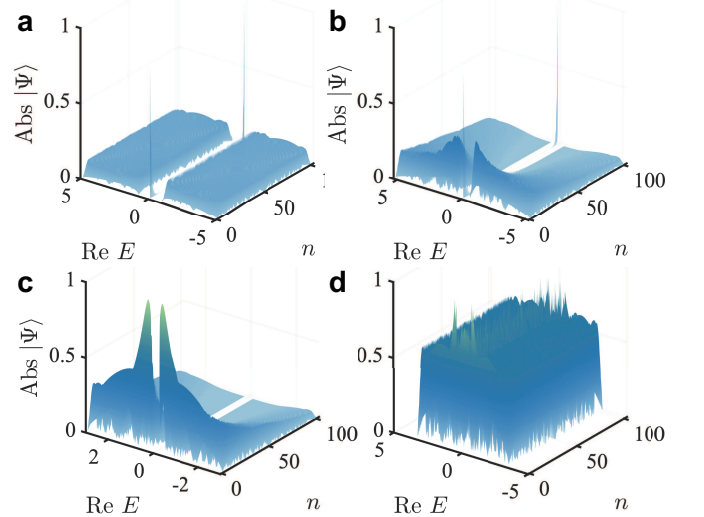


FIG. 2. **Numerical results on the absolute value of eigenstates $|\Psi\rangle$ in non-Hermitian open systems.** $|\Psi\rangle$ is as a function of real part of eigenvalues and cell position n , with lattice size $N = 100$ and on-site energy $\varepsilon_0 = 0$. (a) Phase I with hopping parameters $t_0 = 1$, $t_{1R} = 3.5$, $t_{1L} = 2.5$, $t_2 = 1$. (b) Phase II with $t_0 = 1$, $t_{1R} = 3.5$, $t_{1L} = 2.5$, $t_2 = 1.3$. (c) Phase III with $t_0 = 1$, $t_{1R} = 1.2$, $t_{1L} = 1.6$, $t_2 = 0.6$. (d) Phase IV with $t_0 = 1$, $t_{1R} = 1.2$, $t_{1L} = 1.6$, $t_2 = 1$.

diagram in our one-dimensional model, several analytical approach should be developed to study topological boundary modes and skin modes individually. In this section, we derived the non-Hermitian winding numbers to predict the phase transition points of topological boundary modes, compared with the numerical results calculated by iterative Green's function method[46].

The non-Hermitian winding numbers method is conveniently used for systems protected by sub-lattice symmetry (SLS). Since sites A and B have the same on-site energy ε_0 , our one-dimensional model is exactly protected by SLS when $\varepsilon_0 = 0$, described as

$$\sigma_z H(k) \sigma_z^{-1} = -H(k), \quad (2)$$

where $H(k)$ is the Bloch Hamiltonian, written as

$$H(k) = \begin{pmatrix} 0 & h_a(k) \\ h_b(k) & 0 \end{pmatrix}, \quad (3)$$

$$h_a(k) = t_0 + t_{1R} e^{-ik} + t_2 e^{-i2k},$$

$$h_b(k) = t_0 + t_{1L} e^{ik} + t_2 e^{i2k}.$$

The crucial principle of the non-Bloch-wave approach is to transform the constraint on boundary condition into a non-Bloch wave vector z , where $z = e^{i\tilde{k}}$ and $\tilde{k} \in \mathbb{C}$. Here, we referred to the criterion on the appearance of topological boundary modes that[37],

$$\exists R \in \mathbb{R}_+, W_a(R)W_b(R) < 0, \quad (4)$$

$$W_{a,b}(R) = \frac{1}{2\pi i} \oint_{|z|=R} d[\ln h_{a,b}(z)],$$

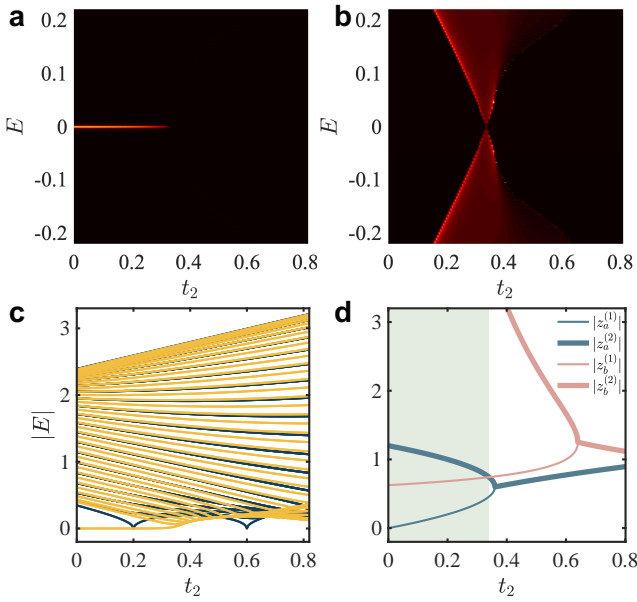


FIG. 3. Phase transition of the topological boundary modes. The hopping parameters are set as $t_0 = 1$, $t_{1R} = 1.2$, $t_{1L} = 1.6$ and $t_2 \in [0, 0.8]$. (a) Surface spectrum function and (b) bulk spectrum function calculated through iterative Green's function method. (c) Numerical results on the eigenvalues of the periodic system and open system with lattice size $N = 40$, denoted by blue and yellow lines respectively. (d) Analytical approach of non-Hermitian winding numbers, where the green region implies the emergence of topological boundary modes.

where $W_{a,b}(R)$ is the so-called non-Hermitian winding number, which is calculated as the number of zeros minus the number of poles encircled by the contour $|z| = R$. Consequently, the existence condition of the topological boundary modes is analytically expressed as,

$$\max\{|z_a^{(1)}|, |z_a^{(2)}|\} > \min\{|z_b^{(1)}|, |z_b^{(2)}|\}. \quad (5)$$

where $z_{a,b}^{(j)}$ are the roots of $h_{a,b}(z) = 0$ respectively (See Supplemental Material Sec. I).

Figure 3 show the numerical and analytical results of topological phase transition in the parameter space t_2 . As shown in Fig. 3(a, b), the calculated surface and bulk spectrum function illustrate that, the topological phase transition point is approximately $t_2 \approx 0.34$ (See Supplemental Material Sec. II). While in Fig. 3(c), the eigenvalues of open system demonstrate that, the topological phase transition point is approximately $t_2 \approx 0.31$. According to Eq. (5), the solution of topological phase transition point is analytically solved as $t_2 = 0.3398$, as shown in Fig. 3(d). Therefore, the analytical result from non-Hermitian winding numbers can precisely predict the numerical results from iterative Green's function method, because non-Bloch-wave approach is established under the thermodynamic limit that $N \rightarrow \infty$.

C. Exact Solution of Non-Hermitian Skin Effects

In this section, we developed the exact solution approach to characterize the non-Hermitian skin modes in our model with long-range couplings. We started with the eigen equation that $\hat{H}|\Psi\rangle = E|\Psi\rangle$, where $|\Psi\rangle = \sum_{n=1}^N [\phi_{n,A}c_{n,A}^\dagger|0\rangle + \phi_{n,B}c_{n,B}^\dagger|0\rangle]$, and $\phi_{n,A/B}$ is the eigenstate on the n^{th} unit cell. Therefore, the recurrence relation about $\phi_{n,A/B}$ is derived as,

$$\begin{aligned} t_0\phi_{n,A} + t_{1L}\phi_{n+1,A} + t_2\phi_{n+2,A} &= (E - \varepsilon_0)\phi_{n,B}, \\ t_2\phi_{n,B} + t_{1R}\phi_{n+1,B} + t_0\phi_{n+2,B} &= (E - \varepsilon_0)\phi_{n+2,A}, \end{aligned} \quad (6)$$

with $n = 1, 2, \dots, N-2$, and the open boundary condition is given by

$$\begin{aligned} t_2\phi_{N+1,A} &= 0, \\ t_{1L}\phi_{N+1,A} + t_2\phi_{N+2,A} &= 0, \\ t_2\phi_{0,B} &= 0, \\ t_{1R}\phi_{0,B} + t_2\phi_{-1,B} &= 0, \end{aligned} \quad (7)$$

which implies that the amplitude of eigenstates vanish outside the 1st to N^{th} unit cells. Assuming that $\phi_{n,A} = \phi_A z^n$ and $\phi_{n,B} = \phi_B z^n$, the nontrivial solution of (ϕ_A, ϕ_B) with $E \neq \varepsilon_0$ requires that

$$(t_0 + t_{1L}z + t_2z^2)(t_2 + t_{1R}z + t_0z^2) = (E - \varepsilon_0)^2z^2. \quad (8)$$

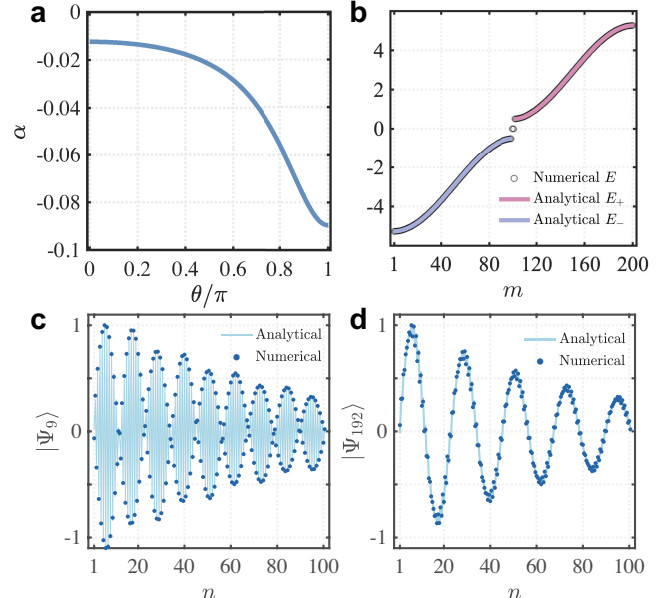


FIG. 4. Exact solution approach to non-Hermitian skin modes for phase II. The hopping parameters are set as $t_0 = 1$, $t_{1R} = 3.5$, $t_{1L} = 2.5$ and $t_2 = 1.3$. (a) Exact solution of localization parameter α as a function of θ described in Eq. (12), where $\theta \in (0, \pi)$ under the thermodynamic limit $N \rightarrow \infty$. (b) Exact solution of the eigenvalues ($E \neq \varepsilon_0$) under open boundary condition, where m denotes the band level. (c, d) Exact solution of the eigenstates, where $m = 9$ in (c), and $m = 192$ in (d).

There are four solutions of z , which satisfy,

$$\begin{aligned} z_1 + z_2 + z_3 + z_4 &= \omega_1, \\ z_1 z_2 + z_1 z_3 + z_1 z_4 + z_2 z_3 + z_2 z_4 + z_3 z_4 &= \omega_2, \\ z_1 z_2 z_3 + z_1 z_2 z_4 + z_1 z_3 z_4 + z_2 z_3 z_4 &= \omega_3, \\ z_1 z_2 z_3 z_4 &= \omega_4, \end{aligned} \quad (9)$$

where

$$\begin{aligned} \omega_1 &= -\frac{t_0 t_{1L} + t_{1R} t_2}{t_0 t_2}, \quad \omega_2 = \frac{t_0^2 + t_{1R} t_{1L} + t_2^2 - (E - \varepsilon_0)^2}{t_0 t_2}, \\ \omega_3 &= -\frac{t_0 t_{1R} + t_{1L} t_2}{t_0 t_2}, \quad \omega_4 = 1. \end{aligned} \quad (10)$$

Therefore, $z_{1,2} = e^{\alpha \pm i\theta}$ and $z_{3,4} = e^{-\alpha \pm i\epsilon}$ with $\alpha \in \mathbb{R}$, and the form of $\phi_{n,A/B}$ is replaced by $\phi_{n,A} = \sum_{j=1}^4 \phi_A^{(j)} z_j^n$ and $\phi_{n,B} = \sum_{j=1}^4 \phi_B^{(j)} z_j^n$. Consequently, under the open boundary condition that $\phi_{N+1,A} = 0$ and $\phi_{0,B} = 0$, we obtained that

$$\sin[(N+1)\theta] + \mu_1 \sin[N\theta] + \mu_2 \sin[(N-1)\theta] = 0, \quad (11)$$

with $\mu_1 = e^{-\alpha} t_{1R}/t_0$ and $\mu_2 = e^{-2\alpha} t_2/t_0$. According to Eq. (9), the parameter α is analytically expressed as

$$\frac{\omega_1 + \omega_3}{\cosh \alpha} + \frac{\omega_1 - \omega_3}{\sinh \alpha} = 8 \cos \theta. \quad (12)$$

θ is continuous among 0 to π under the thermodynamic limit $N \rightarrow \infty$. Finally, the expression of eigenstates with $E \neq \varepsilon_0$ is written as

$$\begin{aligned} |\Psi\rangle &= \sum_{n=1}^N e^{\alpha n} \{ (\sin[n\theta] + \mu_1 \sin[(n-1)\theta] + \mu_2 \sin[(n-2)\theta]) \\ &\quad c_{n,A}^\dagger |0\rangle + \frac{E - \varepsilon_0}{t_0} \sin[n\theta] c_{n,B}^\dagger |0\rangle \}. \end{aligned} \quad (13)$$

α is exactly the localization parameter of eigenstates. Therefore, non-Hermitian skin effects appear as long as $\alpha \neq 0$. When $\alpha < 0$ (> 0), the skin modes are localized at $n = 1$ ($n = N$) side with penetration length $|1/\alpha|$.

As shown in Fig. 4(a), for the case belonging to phase II, the localization parameter α varies with θ , where $\theta \in (0, \pi)$. The exact solution to the eigenvalues and eigenstates are shown in Fig. 4(b) and Fig. 4(c, d) respectively, and the numerical and analytical results correspond to each other precisely.

D. Phase diagram

In our lattice model, the non-Hermitian winding numbers and exact solution approach provide the exact expression of the existence condition of topological boundary modes and skin modes, respectively. Therefore, the four-fold non-Hermitian phase diagram is quickly established through the combination of two methods, as shown in Fig. 5. Compared with other analytical approach, the

exact solution approach holds the advantage that it can provide the exact expression of localization parameter, while the GBZ method relies on the numerical calculation of generalized Brillouin Zone to predict the skin modes (See Supplemental Material Sec. III). We also found that NHSE vanishes if $t_0 = t_2$, as illustrated by phase I and IV, because $\alpha = 0$ when $\omega_1 = \omega_3$. The pseudo-Hermitian symmetry plays a significant role in this situation (See Supplemental Material Sec. IV).

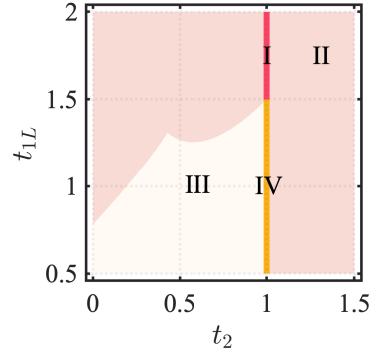


FIG. 5. **Four-fold phase diagram of our non-Hermitian model.** Phase I exhibits topological boundary modes, phase II exhibits both topological boundary modes and skin modes, phase III exhibits skin modes, and phase IV cannot exhibit boundary behaviors, where $t_0 = 1$ and $t_{1R} - t_{1L} = 0.5$.

Our exact solution approach also reveals the intrinsic difference between topological modes and skin modes by further calculation on the number of solvable solutions M . On one hand, the expression of eigenstates illustrates that the $2M$ non-Hermitian skin modes are purely evolved from the bulk states. On the other hand, the topological boundary modes appear because the Hamiltonian becomes singular if $M < N$ under the open boundary condition, so the topological boundary modes are unrelated to the bulk states. According to Eq. (11), the values of μ_1, μ_2 determine the number of roots during $(0, \pi)$. If θ takes $N-1$ or $N-2$ real values, then there exists 2 or 4 topological boundary modes, while the topological modes cannot appear if θ takes N real values. We also found that biorthogonal polarization can predict the number of topological boundary modes when $t_0 \neq t_2$, but fails when $t_0 = t_2$ (See Supplemental Material Sec. V).

E. The modified Lee model

Here, to verify the generality and benefits of our exact solution approach, we proposed a more complicated non-Hermitian model without sub-lattice symmetry, which is modified from Lee model[15] (See Supplemental Material Sec. VI). As shown in Fig. 6(a), each atom is coupled with 5 neighboring atoms, and the interaction between atoms are non-reciprocal, leading to 10 degrees of

freedom. Through the derivation of exact solution approach, the sufficient and necessary condition of the non-existence of non-Hermitian skin effects is given by,

$$\begin{cases} t_{1L}t_{2L} + t_{3R}t_{4R} = t_{1R}t_{2R} + t_{3L}t_{4L} \\ t_{1L} + t_{2L} = t_{1R} + t_{2R} \\ t_{0L}t_{3R} + t_{0R}t_{4R} = t_{0R}t_{3L} + t_{0L}t_{4L} \end{cases}. \quad (14)$$

As shown in Fig. 6(b,c), the eigenstates are delocalized when $t_{4L} = 0.5$, while the non-Hermitian skin effects appear when $t_{4L} = 0.9$, which is consistent with the analytical results in Eq. (14).

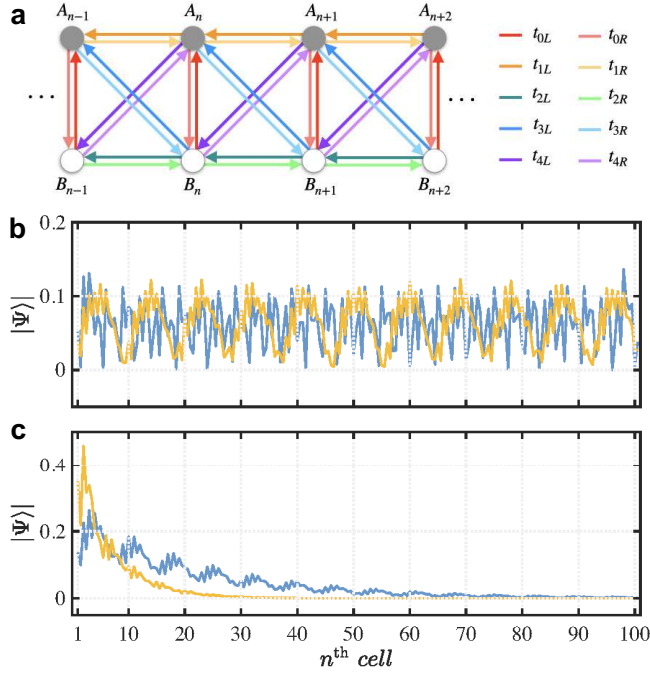


FIG. 6. (a) Schematic view of the modified Lee model without sub-lattice symmetry, where the non-reciprocal hopping parameters are all real numbers, and the on-site energy is ε_0 . (b,c) The numerical results of eigenstates under open boundary condition. The hopping parameters are set as $t_{0L} = 1$, $t_{0R} = 0.5$, $t_{1L} = 1.2$, $t_{1R} = 0.6$, $t_{2L} = 0.6$, $t_{2R} = 1.2$, $t_{3L} = 3$, $t_{3R} = 1.5$, $t_{4R} = 1$ and (b) $t_{4L} = 0.5$; (c) $t_{4L} = 0.9$.

III. CONCLUSIONS

In summary, we successfully presented the four-fold non-Hermitian phase diagram quickly by combining the non-Hermitian winding numbers and exact solution approach, where both the existence condition of topological boundary modes, and the localization length of skin modes are analytically expressed. The general benefits have been proved in a more complicated non-Hermitian Su-Schrieffer-Heeger chain with long-range couplings, providing an efficient routine to study various non-Hermitian phases.

IV. METHODS

A. Derivation of exact solution approach

Here, we provided the detailed derivation of exact solution approach for the non-Hermitian SSH chain with long-range couplings. According to Eq. (8), the boundary condition becomes

$$\begin{cases} \phi_A^{(1)}z_1^{N+1} + \phi_A^{(2)}z_2^{N+1} + \phi_A^{(3)}z_3^{N+1} + \phi_A^{(4)}z_4^{N+1} = 0 \\ \phi_B^{(1)} + \phi_B^{(2)} + \phi_B^{(3)} + \phi_B^{(4)} = 0 \end{cases}. \quad (15)$$

The relation between $\phi_A^{(j)}$ and $\phi_B^{(j)}$ is described as

$$\frac{\phi_B^{(j)}}{\phi_A^{(j)}} = \frac{E - \varepsilon_0}{t_0 + t_{1R}z_j^{-1} + t_2z_j^{-2}}, \quad E \neq \varepsilon_0. \quad (16)$$

Therefore, the nontrivial solution of $(\phi_A^{(1)}, \phi_A^{(2)}, \phi_A^{(3)}, \phi_A^{(4)})$ requires that, there is at least one pair of complex roots (z_i, z_j) that satisfy

$$z_i^{N+1}(t_0 + t_{1R}z_i^{-1} + t_2z_i^{-2}) = z_j^{N+1}(t_0 + t_{1R}z_j^{-1} + t_2z_j^{-2}), \quad (17)$$

where $|z_i| = |z_j|$ under the limitation that $N \rightarrow \infty$. Therefore, the form of $z^{(j)}$ can be rewritten as $z_{1,2} = e^{\alpha \pm i\theta}$, $z_{3,4} = e^{-\alpha \pm i\xi}$ with $\alpha \in \mathbb{R}$, $\theta \in (0, \pi)$, and $\xi \in (0, \pi)$ or $\xi \in i\mathbb{R}$, which means $z_{1,2}$ is a pair of complex roots, and $z_{3,4}$ may be complex pairs or real roots. Accordingly, if $\xi \in i\mathbb{R}$, only $z_{1,2}$ can survive, thus $\phi_A^{(1)}, \phi_A^{(2)} \neq 0$, $\phi_A^{(3)} = \phi_A^{(4)} = 0$. By inserting the form of z into Eq. (9), the relation between α, θ, ξ, E is derived as

$$\begin{aligned} 2e^\alpha \cos \theta + 2e^{-\alpha} \cos \xi &= \omega_1, \\ 2e^\alpha \cos \xi + 2e^{-\alpha} \cos \theta &= \omega_3, \\ 2 \cosh \alpha + 4 \cos \theta \cos \xi &= \frac{t_0^2 + t_{1R}t_{1L} + t_2^2 - (E - \varepsilon_0)^2}{t_0 t_2}. \end{aligned} \quad (18)$$

If $\alpha \neq 0$, the relation of (α, θ) and (α, ξ) are derived as

$$\begin{aligned} \frac{\omega_1 + \omega_3}{\cosh \alpha} + \frac{\omega_1 - \omega_3}{\sinh \alpha} &= 8 \cos \theta, \\ \frac{\omega_1 + \omega_3}{\cosh \alpha} - \frac{\omega_1 - \omega_3}{\sinh \alpha} &= 8 \cos \xi. \end{aligned} \quad (19)$$

Therefore, α can be analytically expressed if $N \rightarrow \infty$. Furthermore, the expression of the eigenvalue E with $E \neq \varepsilon_0$ is described as

$$\begin{aligned} E &= \varepsilon_0 \pm \sqrt{t_0^2 + t_{1R}t_{1L} + t_2^2 - t_0 t_2 f_\alpha}, \\ f_\alpha &= 2 \cosh 2\alpha + \frac{1}{16} \left[\left(\frac{\omega_1 + \omega_3}{\cosh \alpha} \right)^2 - \left(\frac{\omega_1 - \omega_3}{\sinh \alpha} \right)^2 \right]. \end{aligned} \quad (20)$$

The relation of $(\phi_A^{(1)}, \phi_A^{(2)}, \phi_B^{(1)}, \phi_B^{(2)})$ is given by

$$\begin{aligned}\frac{\phi_B^{(2)}}{\phi_B^{(1)}} &= -1, \\ \frac{\phi_B^{(1)}}{\phi_A^{(1)}} &= \frac{E - \varepsilon_0}{t_0 + t_{1R}z_1^{-1} + t_2z_1^{-2}}, \\ \frac{\phi_A^{(2)}}{\phi_A^{(1)}} &= -\frac{t_0 + t_{1R}z_2^{-1} + t_2z_2^{-2}}{t_0 + t_{1R}z_1^{-1} + t_2z_1^{-2}}.\end{aligned}\quad (21)$$

Consequently, the expression of $\phi_{n,A}$ with $E \neq \varepsilon_0$ is derived as

$$\begin{aligned}\phi_{n,A} &= \phi_A^{(1)}z_1^n + \phi_A^{(2)}z_2^n \\ &= \phi_A^{(1)}[z_1^n - \frac{t_0 + t_{1R}z_2^{-1} + t_2z_2^{-2}}{t_0 + t_{1R}z_1^{-1} + t_2z_1^{-2}}z_2^n] \\ &= \frac{2i\phi_A^{(1)}t_0}{t_0 + t_{1R}z_1^{-1} + t_2z_1^{-2}}e^{\alpha n}\{\sin[n\theta] + \mu_1 \sin[(n-1)\theta] \\ &\quad + \mu_2 \sin[(n-2)\theta]\},\end{aligned}\quad (22)$$

The expression of $\phi_{n,B}$ with $E \neq \varepsilon_0$ is derived as

$$\begin{aligned}\phi_{n,B} &= \phi_B^{(1)}z_1^n + \phi_B^{(2)}z_2^n \\ &= \frac{2i\phi_A^{(1)}(E - \varepsilon_0)}{t_0 + t_{1R}z_1^{-1} + t_2z_1^{-2}}e^{\alpha n}\sin[n\theta].\end{aligned}\quad (23)$$

- [1] A. Mostafazadeh, Pseudo-hermiticity versus PT symmetry: The necessary condition for the reality of the spectrum of a non-Hermitian Hamiltonian, *J. Math. Phys.* **43**, 205 (2002).
- [2] C. M. Bender, Making sense of non-Hermitian Hamiltonians, *Rep. Prog. Phys.* **70**, 947 (2007).
- [3] R. El-Ganainy, K. G. Makris, M. Khajavikhan, Z. H. Musslimani, S. Rotter, and D. N. Christodoulides, Non-Hermitian physics and PT symmetry, *Nat. Phys.* **14**, 11 (2018).
- [4] Z. Gong, Y. Ashida, K. Kawabata, K. Takasan, S. Higashikawa, and M. Ueda, Topological Phases of non-Hermitian systems, *Phys. Rev. X* **8**, 031079 (2018).
- [5] A. Ghatak and T. Das, New topological invariants in non-Hermitian systems, *J. Phys.: Condens. Matter* **31**, 263001 (2019).
- [6] Y. Ashida, Z. Gong, and M. Ueda, Non-Hermitian physics, *Adv. Phys.* **69**, 249 (2020).
- [7] E. J. Bergholtz, J. C. Budich, and F. K. Kunst, Exceptional topology of non-Hermitian systems, *Rev. Mod. Phys.* **93**, 015005 (2021).
- [8] B. A. Bernevig, T. L. Hughes, and S.-C. Zhang, Quantum spin Hall effect and topological phase transition in HgTe quantum wells, *Science* **314**, 1757 (2006).
- [9] A. P. Schnyder, S. Ryu, A. Furusaki, and A. W. W. Ludwig, Classification of topological insulators and superconductors in three spatial dimensions, *Phys. Rev. B* **78**, 195125 (2008).
- [10] K. v. Klitzing, G. Dorda, and M. Pepper, New method for high-accuracy determination of the fine-

Because α is the localization parameter of the eigenstates, the non-existence of NHSE requires that

$$\forall \theta \in (0, \pi), \alpha = 0. \quad (24)$$

By inserting Eq. (24) into Eq. (18), we obtained that $\omega_1 = \omega_3$. Therefore, the NHSE vanishes if and only if $t_0 = t_2$ or $t_{1L} = t_{1R}$.

DATA AVAILABILITY

The data that support the plots within this paper and other findings of this study are available from the corresponding author on reasonable request.

CODE AVAILABILITY

The computer codes used to generate the data presented in the manuscript are available from the corresponding author on reasonable request.

- structure constant based on quantized Hall resistance, *Phys. Rev. Lett.* **45**, 494 (1980).
- [11] D. J. Thouless, M. Kohmoto, M. P. Nightingale, and M. den Nijs, Quantized Hall conductance in a two-dimensional periodic potential, *Phys. Rev. Lett.* **49**, 405 (1982).
- [12] Y. Hatsugai, Chern number and edge states in the integer quantum Hall effect, *Phys. Rev. Lett.* **71**, 3697 (1993).
- [13] Y. Xiong, Why does bulk boundary correspondence fail in some non-Hermitian topological models, *J. Phys. Commun.* **2**, 035043 (2018).
- [14] H. Wang, J. Ruan, and H. Zhang, Non-Hermitian nodal-line semimetals with an anomalous bulk-boundary correspondence, *Phys. Rev. B* **99**, 075130 (2019).
- [15] T. E. Lee, Anomalous edge state in a non-Hermitian lattice, *Phys. Rev. Lett.* **116**, 133903 (2016).
- [16] V. M. Martinez Alvarez, J. E. Barrios Vargas, and L. E. F. Foa Torres, Non-Hermitian robust edge states in one dimension: Anomalous localization and eigenspace condensation at exceptional points, *Phys. Rev. B* **97**, 121401 (2018).
- [17] N. Okuma, K. Kawabata, K. Shiozaki, and M. Sato, Topological origin of non-Hermitian skin effects, *Phys. Rev. Lett.* **124**, 086801 (2020).
- [18] K. Yokomizo and S. Murakami, Scaling rule for the critical non-Hermitian skin effect, *Phys. Rev. B* **104**, 165117 (2021).
- [19] K.-M. Kim and M. J. Park, Disorder-driven phase transition in the second-order non-Hermitian skin effect, *Phys. Rev. B* **104**, L121101 (2021).

[20] X. Zhu, H. Wang, S. K. Gupta, H. Zhang, B. Xie, M. Lu, and Y. Chen, Photonic non-Hermitian skin effect and non-Bloch bulk-boundary correspondence, *Phys. Rev. Research* **2**, 013280 (2020).

[21] J. Zhong, K. Wang, Y. Park, V. Asadchy, C. C. Wojcik, A. Dutt, and S. Fan, Nontrivial point-gap topology and non-Hermitian skin effect in photonic crystals, *Phys. Rev. B* **104**, 125416 (2021).

[22] X. Zhang, Y. Tian, J.-H. Jiang, M.-H. Lu, and Y.-F. Chen, Observation of higher-order non-Hermitian skin effect, *Nat. Commun.* **12**, 5377 (2021).

[23] T. Yoshida, T. Mizoguchi, and Y. Hatsugai, Mirror skin effect and its electric circuit simulation, *Phys. Rev. Research* **2**, 022062 (2020).

[24] T. Hofmann, T. Helbig, F. Schindler, N. Salgo, M. Brzezińska, M. Greiter, T. Kiessling, D. Wolf, A. Vollhardt, A. Kabaši, C. H. Lee, A. Bilušić, R. Thomale, and T. Neupert, Reciprocal skin effect and its realization in a topoelectrical circuit, *Phys. Rev. Research* **2**, 023265 (2020).

[25] K. Xu, X. Zhang, K. Luo, R. Yu, D. Li, and H. Zhang, Coexistence of topological edge states and skin effects in the non-Hermitian Su-Schrieffer-Heeger model with long-range nonreciprocal hopping in topoelectric realizations, *Phys. Rev. B* **103**, 125411 (2021).

[26] X. Zhang, K. Xu, C. Liu, X. Song, B. Hou, R. Yu, H. Zhang, D. Li, and J. Li, Gauge-dependent topology in non-reciprocal hopping systems with pseudo-Hermitian symmetry, *Commun. Phys.* **4**, 166 (2021).

[27] D. Zou, T. Chen, W. He, J. Bao, C. H. Lee, H. Sun, and X. Zhang, Observation of hybrid higher-order skin-topological effect in non-Hermitian topoelectrical circuits, *Nat. Commun.* **12**, 7201 (2021).

[28] L. Zhang, Y. Yang, Y. Ge, Y.-J. Guan, Q. Chen, Q. Yan, F. Chen, R. Xi, Y. Li, D. Jia, S.-Q. Yuan, H.-X. Sun, H. Chen, and B. Zhang, Acoustic non-Hermitian skin effect from twisted winding topology, *Nat. Commun.* **12**, 6297 (2021).

[29] L. Xiao, T. Deng, K. Wang, G. Zhu, Z. Wang, W. Yi, and P. Xue, Non-Hermitian bulk-boundary correspondence in quantum dynamics, *Nat. Phys.* **16**, 761 (2020).

[30] C. Yin, H. Jiang, L. Li, R. Lü, and S. Chen, Geometrical meaning of winding number and its characterization of topological phases in one-dimensional chiral non-Hermitian systems, *Phys. Rev. A* **97**, 052115 (2018).

[31] H. Shen, B. Zhen, and L. Fu, Topological band theory for non-Hermitian Hamiltonians, *Phys. Rev. Lett.* **120**, 146402 (2018).

[32] S. Yao, F. Song, and Z. Wang, Non-Hermitian Chern bands, *Phys. Rev. Lett.* **121**, 136802 (2018).

[33] S. Yao and Z. Wang, Edge states and topological invariants of non-Hermitian systems, *Phys. Rev. Lett.* **121**, 086803 (2018).

[34] Z. Yang, K. Zhang, C. Fang, and J. Hu, Non-Hermitian bulk-boundary correspondence and auxiliary generalized Brillouin Zone theory, *Phys. Rev. Lett.* **125**, 226402 (2020).

[35] K. Yokomizo and S. Murakami, Non-Bloch band theory of non-Hermitian systems, *Phys. Rev. Lett.* **123**, 066404 (2019).

[36] K. Kawabata, N. Okuma, and M. Sato, Non-Bloch band theory of non-Hermitian Hamiltonians in the symplectic class, *Phys. Rev. B* **101**, 195147 (2020).

[37] C. H. Lee and R. Thomale, Anatomy of skin modes and topology in non-Hermitian systems, *Phys. Rev. B* **99**, 201103 (2019).

[38] D. S. Borgnia, A. J. Kruchkov, and R.-J. Slager, Non-Hermitian boundary modes and topology, *Phys. Rev. Lett.* **124**, 056802 (2020).

[39] K. Zhang, Z. Yang, and C. Fang, Correspondence between winding numbers and skin modes in non-Hermitian systems, *Phys. Rev. Lett.* **125**, 126402 (2020).

[40] F. K. Kunst, E. Edvardsson, J. C. Budich, and E. J. Bergholtz, Biorthogonal bulk-boundary correspondence in non-Hermitian systems, *Phys. Rev. Lett.* **121**, 026808 (2018).

[41] E. Edvardsson, F. K. Kunst, and E. J. Bergholtz, Non-Hermitian extensions of higher-order topological phases and their biorthogonal bulk-boundary correspondence, *Phys. Rev. B* **99**, 081302 (2019).

[42] E. Edvardsson, F. K. Kunst, T. Yoshida, and E. J. Bergholtz, Phase transitions and generalized biorthogonal polarization in non-Hermitian systems, *Phys. Rev. Research* **2**, 043046 (2020).

[43] C.-X. Guo, C.-H. Liu, X.-M. Zhao, Y. Liu, and S. Chen, Exact solution of non-Hermitian systems with generalized boundary conditions: Size-dependent boundary effect and fragility of the skin effect, *Phys. Rev. Lett.* **127**, 116801 (2021).

[44] Y. Liu, Y. Zeng, L. Li, and S. Chen, Exact solution of the single impurity problem in nonreciprocal lattices: Impurity-induced size-dependent non-Hermitian skin effect, *Phys. Rev. B* **104**, 085401 (2021).

[45] F. K. Kunst and V. Dwivedi, Non-Hermitian systems and topology: A transfer-matrix perspective, *Phys. Rev. B* **99**, 245116 (2019).

[46] M. P. L. Sancho, J. M. L. Sancho, J. M. L. Sancho, and J. Rubio, Highly convergent schemes for the calculation of bulk and surface green functions, *J. Phys. F: Met. Phys.* **15**, 851 (1985).

ACKNOWLEDGMENTS

The authors thank for the support from the National Natural Science Foundation of China (Grant Nos. 60578047, 61427815), and the Natural Science Foundation of Shanghai (Grant Nos. 17ZR1402200, 13ZR1402600).

AUTHOR CONTRIBUTIONS

J. Li contributed to the plan of the project. X. Zhang contributed to the numerical and analytical calculations. X. Song, S. Zhang, T. Zhang, Y. Liao and X. Cai helped to improve the design of lattice models. All authors participated in the discussion on the results, and have read and agreed the published version of the manuscript.

COMPETING INTERESTS

The authors declare no competing interests.